https://doi.org/10.5194/egusphere-2023-2662
Preprint. Discussion started: 20 November 2023

Aqueous-phase chemistry of glyoxal with multifunctional reduced nitrogen compound: A potential missing route of secondary brown carbon

Yuemeng Ji[1,2], Zhang Shi[1,2], Wenjian Li[1,2], Jiaxin Wang[1,2], Qiuju Shi[1,2], Yixin Li[3], Lei Gao[1,2], Ruize Ma[1,2], Weijun Lu[2], Lulu Xu[1,2], Yanpeng Gao[1,2], Guiying Li[1,2], Taicheng An[1,2]

[1]Guangdong Key Laboratory of Environmental Catalysis and Health Risk Control, Guangdong-Hong Kong-Macao Joint Laboratory for Contaminants Exposure and Health, Institute of Environmental Health and Pollution control, Guangdong University of Technology, Guangzhou 510006, China;
[2]Guangzhou Key Laboratory of Environmental Catalysis and Pollution Control, Key Laboratory of City Cluster Environmental Safety and Green Development, School of Environmental Science and Engineering, Guangdong University of Technology, Guangzhou 510006, China.
[3]Department of Chemistry, University of California Irvine, Irvine, CA 92697, USA

Correspondence to: Prof. Taicheng An (antc99@gdut.edu.cn)

Abstract. Aqueous-phase chemistry of glyoxal (GL) with reduced nitrogen compounds (RNCs) plays a significant source of secondary brown carbon (SBrC), which is one of the largest uncertainties in climate predictions. However, few studies have revealed that SBrC formation is affected by multifunctional RNCs, which has a non-negligible atmospheric abundance. Hence, we performed theoretical and experimental approaches to investigate the reaction mechanisms and kinetics of the mixtures for ammonium sulfate (AS), multifunctional amine (monoethanolamine, MEA) and GL. Our experiments indicate that the light-absorption and the growth rate are enhanced in MEA-GL mixture relative to AS-GL and MEA-AS-GL mixtures, and MEA reactions of the chromophores by more efficiently than the analogous AS reactions. Quantum chemical calculations show that the formation and propagation of oligomers proceed via four-step nucleophilic addition reactions in three reaction systems. The presence of MEA provides the extra two branched chains to affect the natural charges and steric hindrance of intermediates, facilitated the formation of chromophores. Molecule dynamics simulations reveal that the interfacial and interior attraction on the aqueous aerosols with MEA is more pronounced for small α-dicarbonyls, to facilitate the further engagement in the aqueous-phase reactions. Our results show a possible missing source for SBrC formation on urban, regional and global scales.

1 Introduction

Brown carbon (BrC) represents the most important source of carbonaceous aerosols, with profound implications to the global climate, air quality and human health (Laskin et al., 2015; Marrero-Ortiz et al., 2018; Li et al., 2022; Yan et al., 2018; Yuan et al., 2023). Chemical transport models reveal that a non-negligible radiative forcing by BrC is range from 0.05 to 0.27 W m^{-2} averaged globally (Tuccella et al., 2020; Wang et al., 2018; De Haan et al., 2020; Zhang et al., 2020; Laskin et al., 2015; Moise et al., 2015). Large differences in these estimated data result from the uncertainties of BrC on its formation mechanisms,

https://doi.org/10.5194/egusphere-2023-2662
Preprint. Discussion started: 20 November 2023

chemical composition and optical properties (An et al., 2019; Shi et al., 2020; Kasthuriarachchi et al., 2020; Corbin et al., 2019). It affects understanding the radiative effect in current climate models (Liu et al., 2020; Zhang et al., 2020; Zhang et al., 2023). Compared with primary BrC, sources and formation of secondary BrC (SBrC) are more complex and lack of understanding in detail (Lin et al., 2015; Yuan et al., 2020; Srivastava et al., 2022). Hence, in recent years, great efforts have been made to better understand the chemical composition and formation mechanisms of SBrC chromophores.

There is compelling evidence that the heterogeneous reactions of reduced nitrogen compounds (RNCs) and small α-dicarbonyls have been recognized as significant sources of SBrC (Hawkins et al., 2018; De Haan et al., 2018; George et al., 2015). These SBrC chromophores are normally conjugated and possibly heteroaromatic species, such as imidazole (IML) and its derivatives (De Haan et al., 2009b; De Haan et al., 2009a; Yang et al., 2022). Numerous previous studies paid much attention to BrC from the secondary processes of small α-dicarbonyls with ammonium sulfate (AS) and methylamine (MA) (De Haan et al., 2020; De Haan et al., 2019; De Haan et al., 2009a; Lin et al., 2015). For example, nearly 30 chromophores were detected in AS-methylglyoxal (MG) mixture by HPLC/PDA/HRMS and nitrogen-containing compounds account for more than 70% of the overall light absorption within 300−500 nm range (Lin et al., 2015). Some studies have also revealed that the absorption of BrC generated in AS- or MA-MG mixture increases with pH value (Hawkins et al., 2018; Sedehi et al., 2013) Also, the iminium pathway is predominant while pH < 4 to form IML and its derivatives but is suppressed at pH 4.(Nozière et al., 2009; Sedehi et al., 2013; Yu et al., 2011). Hence, pH value has a large effect on the formation of SBrC chromophores, but the chemical mechanisms of BrC formation under the different pH values remain unclear, hindering a systematical understanding its integrated atmospheric chemistry and nonnegligible environmental impacts.

On the other hand, multifunctional RNCs (such as ethanolamines and amino acids) display a strong atmospheric activity to the formation of SBrC with an unneglected atmospheric concentration (Huang et al., 2016; Ge et al., 2011; Powelson et al., 2014; Trainic et al., 2012; Laskin et al., 2015; Ning et al., 2022). For example, a rapid BrC formation was detected in glycine reactions with small α-dicarbonyls, and sub-micrometer amino acids particles exhibited a high growth upon exposure to small α-dicarbonyls (Powelson et al., 2014; Sedehi et al., 2013; De Haan et al., 2009b; Trainic et al., 2012). On the other hand, monoethanolamine (MEA) is an amine-based solvent for post-combustion CO_2 capture (PCCC) technology with a relatively high vapor pressure, emitting 80 tons per year into the atmosphere for each 1 million tons of CO_2 removed per year (Karl et al., 2011; Puxty et al., 2009; Shen et al., 2019). Recent field measurement has shown that MEA is the second most abundant organic amine in $PM_{2.5}$ in Shanghai besides MA (Huang et al., 2016). However, to the best of our knowledge, few previous results are available on the participation of MEA in the SBrC formation with small α-dicarbonyls and its potential role in the atmosphere and human health were also not attempted.

Hence, we elucidated the chemical mechanisms of BrC chromophores from the mixtures of typical reaction of RCNs (i.e., MEA and AS) with small α-dicarbonyls using combined theoretical and experimental methods. Herein, glyoxal (GL) is selected as the representative of small α-dicarbonyls due to its high global emissions and significant contribution to BrC (Fu et al., 2008; Myriokefalitakis et al., 2008; Shi et al., 2020; Nie et al., 2022; Gomez et al., 2015). The chemical composition of the BrC chromophores was characterized by mass spectrometry in different initial pH values, and the optical properties were

https://doi.org/10.5194/egusphere-2023-2662
Preprint. Discussion started: 20 November 2023

measured using UV-Vis spectrophotometry. Possible pathways were calculated using density functional theory, and the mechanism of BrC chromophore formation was also simulated. The effects of multifunctional amines in formation of SBrC chromophores were elaborated further. Additionally, the potential implications of multifunctional amines on climate radiative forcing were stated and discussed briefly.

2 Experimental methods and theoretical calculations

2.1 Experimental section

The procedures of each experiment are summarized in Fig. S1. All reagents were used as described in Supporting Information (SI). Three mixtures were prepared under atmospheric relevant aqueous conditions to generate SBrC: AS-GL, MEA-GL and MEA-AS-GL. Briefly, AS-GL (1 M) mixture was prepared by adding AS to aqueous GL (in ultrapure water) for a final concentration of 1 M of each reactant in the volumetric flasks. For the two MEA-containing mixtures, MEA was acidified with diluted sulfuric acid (20%) to prevent GL from reacting with MEA in alkaline condition. The acidified MEA was then combined with aqueous GL similar to that described for the AS-GL (1 M) mixture. All three solutions mentioned above were then diluted to reach a final concentration of 1 M in three 50mL volumetric flasks. To explore the effects of pH values, three mixtures were prepared with an initial pH values of 3 or 4 via addition of sulfuric acid (20%) or sodium hydroxide solution (2 M) prior to the mixing of RNCs and GL (Kampf et al., 2016; Yu et al., 2011). Each mixture was then transported into brown vials for 15 days in dark condition, which has been proved efficient formation of chromophores in droplet evaporation collecting on the timescales of seconds (Zhao et al., 2015; Lee et al., 2014).

The absorption spectrums of all mixtures were recorded by using an UV-Vis spectrophotometer (Agilent Cary 300, USA). All experimental solutions were diluted by a factor of 200 or 400 before each measurement to avoid saturation of the absorption peaks. The diluted samples were added into a quartz cuvette with 1 cm optical path length right away to prevent the diluted samples from photolysis. The spectrums recorded between 200 – 500 nm were shown in Fig. 1. And the blank experiments of GL and RNCs solution were performed and presented in Fig. S2. The absorption spectrums of all samples were measured with three times. The wavelength-dependent mass absorption coefficients (MACs) of experimental solutions were calculated from initial base-10 absorbance (A_{10}),

$$\mathrm{MAC}(\lambda) = \frac{A_{10}^{\mathrm{solution}}(\lambda) \times \ln(10)}{b \times C_{\mathrm{mass}}}$$

where C_{mass} is the mass concentration of reactants and b is path length (Aiona et al., 2017; Chen and Bond, 2010). The different dilution factors were normalized by using MAC formula.

Samples used for mass spectrometry analysis were diluted by a factor of 800 or 1000 followed by syringe filtration. The filters were stored in brown chromatography injection vials to block the light. Ultra-performance liquid chromatography coupled to hybrid Quadrupole-Exactive Orbitrap mass spectrometry (UPLC-Q-Orbitrap HRMS, Thermo Scientific™, USA) (Wang et al., 2017) was employed to obtain structural data of chromophores in this study. MS^2 analysis were used for all

https://doi.org/10.5194/egusphere-2023-2662
Preprint. Discussion started: 20 November 2023

chromophores with a weight error of less than 10 ppm compared with the theoretical mass to obtain fragments information for the identification of structure analysis. Detailed description of the mass spectrometry and chromatographic conditions are all described in SI.

2.2 Quantum calculations and molecular dynamics simulations

Quantum chemical calculations were performed using the Gaussian 09 package (M. J.Frisch, 2013). Structures for all stationary points (SPs), including reactants, intermediates, transient states (TSs), and products, were optimized using the hybrid density functional of M06-2X method(Zhao and Truhlar, 2007) with 6-311G(d,p) basis set, i.e., at the M06-2X/6-311G(d,p) level (Ji et al., 2017). The solvent effect was considered using the solvation model based on density (SMD) to simulate the aqueous environment (Gao et al., 2016; Marenich et al., 2009). Harmonic frequency calculation was carried out at the same level as structural optimization to verify whether SP is a TS (with one and only imaginary frequency) or a minimum (without imaginary frequencies) (Ji et al., 2022). Intrinsic reaction coordinate calculation was performed to confirm that the TSs connected with the corresponding reactants and products. Single point energy (SPE) calculation was executed using the M06-2X method with a more flexible 6-311+G(3df,3pd) basis set to obtain more accurate potential energy surfaces (PESs). For the pathways with TSs, the rate constants (k) were calculated via conventional transition state theory (TST) (Evans and Polanyi, 1935; Eyring, 1935; Galano and Alvarez-Idaboy, 2009; Gao et al., 2014). To simulate real atmospheric conditions in the solution, the calculated k values were refined by solvent cage effects(Okuno, 1997) and diffusion-limited effects (Collins and Kimball, 1949), of which the calculation details of diffusion-limited rate constant k_d can be seen in SI. For the pathways without TSs, the corresponding k values are predominated by the diffusion-limit effect which equal to the diffusion-limited rate constants.

Classical molecular dynamics (MD) was performed using NAMD package (Phillips et al., 2005) to simulate the heterogeneous processes of GL from gas to the AS and MEA particles. The AS particle is composed of 39 SO_4^{2-}, 78 NH_4^+ and 2046 H_2O in a box size of 40 × 40 × 40 $Å^3$, while the MEA particle consists of 39 MEA and 2036 H_2O. The 5 ns equilibration at the time step of 1 fs was executed in the isothermal-isochoric (NVT) ensemble (T = 298 K) to ensure the thermodynamic equilibrium of particles (Shi et al., 2020; Zhang et al., 2019). The MD simulation of 2 ns is run via the NVT ensemble. MEA and GL were described using CHARMM force field (Jorgensen et al., 1996), and H_2O using TIP3P model (Martins-Costa et al., 2012). The fixed charges on NH_4^+ and SO_4^{2-} are scaled by 0.75 to account for the electronic polarizability (Leontyev and Stuchebrukhov, 2011; Mosallanejad et al., 2020). The periodic boundary conditions were selected for three dimensions. In order to calculate the kinetic trajectories of GL from gas to two target particles, the free energy profile along the distance of the center of mass between each particle and GL was calculated via umbrella sampling (Torrie and Valleau, 1977) and weighted-histogram analysis method (Kumar et al., 1992) based on the above equilibrated molecular dynamics trajectories. The bias potential force constant was equal to 10 kcal mol^{-1} $Å^{-2}$.

https://doi.org/10.5194/egusphere-2023-2662
Preprint. Discussion started: 20 November 2023

3 RESULTS AND DISCUSSION

3.1 Mass absorption coefficients of BrC chromophores

The mass absorption coefficients (MACs) identified in AS-GL, MEA-GL, and MEA-AS-GL mixtures at the initial pH of 3 and 4 (denoted as pH = 3 and pH = 4) are shown in Fig. S3. The maximum adsorption peaks locate at 207, 212, and 209 nm for AS-GL, MEA-GL, and MEA-AS-GL mixtures at pH = 3, respectively, which are the characteristic of BrC chromophores. Also the corresponding location is not changed at pH = 4. The MAC values of the maximum adsorption peaks are in the range of 1080−17909 $cm^2\ g^{-1}$ for three mixtures, which are quantitatively similar to other aerosol samples generated in laboratory smog chambers with MACs of SBrC on the order of ~10^{2-4} $cm^2\ g^{-1}$ (Ackendorf et al., 2017; Kampf et al., 2016; Lee et al., 2013; Powelson et al., 2014; Shapiro et al., 2009; Yu et al., 2011; Zhao et al., 2015). The MAC values at pH = 4 are higher than those at pH = 3 for three mixtures. For example, the MAC value in AS-GL mixture is 2037 $cm^2\ g^{-1}$ at pH = 4, which is almost twice higher than that at pH = 3. Hence, the initial pH values of solution mainly affect the MAC values rather than the locations of absorption peaks.

Fig. 1a shows a comparison of the MAC values of all three mixtures at the initial pH of 3 and 4. The MAC values of maximum adsorption peaks increase from AS-GL to MEA-GL to MEA-AS-GL mixture, ranging from 1080 to 6345 $cm^2\ g^{-1}$ at pH = 3 and 2037 to 7617 $cm^2\ g^{-1}$ at pH = 4. The highest MAC value of MEA-AS-GL is explained by the different initial total concentration of reactants (see in Method), since the initial concentration of AS and MEA in MEA-AS-GL mixture is twice times than that in MEA-GL or AS-GL mixture. In addition, the MAC value of maximum adsorption peak in MEA-AS-GL mixture is higher than the sum of those in MEA-GL and AS-GL mixtures, and the location of maximum absorption peak in MEA-AS-GL mixture is between those in MEA-GL and AS-GL mixtures. It implies that the extra chromophores are yielded in MEA-AS-GL mixture in addition to producing the same chromophores as AS-GL and MEA-GL mixtures.

To compare the formation rate of chromophore between the different mixtures, the growth rates (GRs) of the maximum absorption peaks as a function of reaction time is shown in Fig. 2. The trend of the GR variation with reaction time at pH = 3 is similar to that at pH = 4, while the GRs of three mixtures at pH = 4 are larger than those at pH = 3 at the beginning of the reactions. The GRs are nearly invariant after 6−9 days, implying that the chromophore formation for three mixtures is irreversible. MEA-AS-GL mixture exhibits the larger GRs than other mixtures at the beginning of reaction because of its higher initial concentration of reactants. As the reaction proceeds, the GRs of MEA-GL mixture are increased and finally larger than those of other mixtures. Hence, MEA reactions form the chromophores by more efficiently than the analogous AS reactions.

The GRs dependence of the pH values of three mixtures is also plotted as a function of reaction time as shown in Fig. 2. The pH values rapidly degrade within the first 2 days in three mixtures, which is the same trend as GRs that decrease by a factor of more than 1−3 at pH = 3 and 4. This trend is explained by ambient pH values, since a known byproduct (i.e., formic acid) is formed (De Haan et al., 2009b; De Haan et al., 2020; Galloway et al., 2009; Hamilton et al., 2013; Kampf et al., 2012; Yu et al., 2011). Note that the trend of GRs shows a decrease from MEA-AS-GL, MEA-GL, to AS-GL mixtures at the beginning of the reaction time, while the MAC values of MEA-GL mixture are larger than those of two mixtures because of the smaller

https://doi.org/10.5194/egusphere-2023-2662
Preprint. Discussion started: 20 November 2023

pH value in solution after the reaction is equilibrium (Figs. 1b and 2), suggesting that chromophore formation of three mixtures depends on the ambient pH value.

3.2 Chemical composition characterization of BrC chromophores

The chemical composition characterization of formed BrC chromophore were conducted by UPLC-Q-Orbitrap HRMS. The formulas, m/z values, characteristic fragments, and structures of chromophores and intermediates are identified based on obtained mass spectrum data in AS-GL, MEA-GL, and MEA-AS -GL mixtures (Table S1). The corresponding MS and MS^2 spectrums of chromophores and intermediates are exhibited in Fig. 3 and Figs. S4-S8. For all mixtures, imidazole (IML) compounds are identified with a characteristic peak at m/z 69.045 in MS^2 spectrums. Therefore, various IML compounds are observed based on several representative peaks at m/z 69.045, including imidazole (IML_{AS} and IML_{MEA}), imidazole-2-carboxaldehyde (IC_{AS} and IC_{MEA}), and their hydrated forms (HIC_{AS} and HIC_{MEA}) for AS-GL and MEA-GL mixtures (Table S1, Figs. 3a-b and S4-S5). For MEA-GL mixture, extra catenulate intermediates without IML-structure characteristics are obtained at m/z values of 102.055 and 120.065 (Table S1, Figs. 3a and S6), corresponding to $C_4H_7O_2N$ (IA_{MEA}) and $C_4H_9O_3N$ (AHA_{MEA} and ID_{MEA}) compounds, respectively. However, no catenulate intermediates in AS-GL mixture are observed in this study because of their low concentrations and short lifetimes, although they are observed by previous studies using MS/AMS and ^1H nuclear magnetic resonance spectroscopy (Galloway et al., 2009; Lee et al., 2013; Yu et al., 2011). In addition, as shown in Fig. 3b and Fig. S7, some IML-based products at m/z values of 145.061, 135.066, and 193.072 were obtained in AS-GL mixture correspond to hydrated N-glyoxal substituted imidazole (HGI_{AS}), 2,2'-biimidazole (BIM_{AS}), and its glyoxal substituted analog (GBI_{AS}), respectively. As discussed above, an important distinction between AS-GL and MEA-GL mixtures is whether formation of bicyclic IML products (Fig. 3a-b), indicating that the optical properties of chromophores are mainly determined by mono-imidazole compounds rather than bicyclic IML compounds.

To further explore the difference of identified products in MEA-GL and AS-GL mixtures, the possible pathways leading to the identified intermediates and chromophores are illustrated in Fig. 4, along with the reaction energies (ΔG_r) of all pathways calculated at the M06-2X/6-311+G(3df,3pd)//M06-2X/6-311G(d,p) level. As shown in Fig. 4, the formation and propagation of oligomers was proposed to proceed via four-step nucleophilic addition (NA) reactions. For MEA-GL mixture, three catenulate intermediates (AHA_{MEA}, IA_{MEA}, and ID_{MEA}) are successively yielded by the nucleophilic attack of MEA at the reactive carbonyl site via dehydration and hydration, with the total ΔG_r value of −7.8 kcal mol^{-1} (Fig. 4a). Subsequently, two-step NA reactions between ID_{MEA} and MEA and between DI_{MEA} and GL-diol (DL), followed by protonation and dehydration, yields two intermediates (HA_{MEA} and PIC_{MEA}) in sequence. Although the third NA reaction between DI_{MEA} and DL is endothermic (ΔG_r = 12.7 kcal mol^{-1}), the total ΔG_r value of DI_{MEA} formation in MEA-GL mixture is −18.7 kcal mol^{-1} for proceeding the NA reaction to yield PIC_{MEA}. Similarly, the formation of PIC_{AS} in AS-GL mixture is also thermodynamically feasible, with the total ΔG_r value of −10.9 kcal mol^{-1}. However, PIC_{MEA} or PIC_{AS} is thermodynamically unstable, since there is a large exothermicity of the subsequent reaction pathway (ΔG_r = −78.6 or −50.0 kcal mol^{-1}) for proceeding cyclization leading to the formation of IC_{MEA} or IC_{AS}. It should be noted that for AS-GL mixture, the fate of IC_{AS} is dependent of the

https://doi.org/10.5194/egusphere-2023-2662
Preprint. Discussion started: 20 November 2023

competition between the pathways of hydration to yield HIC_{AS} and NA reaction with DL to form BI_{AS}, while for MEA-GL mixture, there are no nucleophilic sites of IC_{MEA} for further oligomerization to form bicyclic IML compounds because IC_{MEA} is imidazolium cation. Current results further explain our experimental results mentioned above that higher MAC and larger GR values in MEA-GL mixture than that in AS-GL mixture.

For MEA-AS-GL mixture, the products in AS-GL and MEA-GL mixtures are also observed (Fig. 3c). Beyond that, four extra IML compounds are also observed at m/z values of 113.071, 141.066, 159.076 and 171.076, corresponding to IML (IML_{MAG}), imidazole-2-carboxaldehyde (IC_{MAG}) and its hydrated form (HIC_{MAG}), and N-glyoxal substituted imidazole (GI_{MAG}) (Fig. 3c and Fig. S8). An extra -C_2H_4O group exists in the geometries of the above four IML compounds relative to the products of AL-GL mixture, indicating that there exist the cross reactions between MEA and AS in the MEA-AS-GL mixture. As shown in Fig. 5, the cross NA reaction between ID_{AS} and MEA or ID_{MEA} and AS possesses a negative ΔG_r value of −4.8 or −5.4 kcal mol^{-1}, followed by dehydration to form the same intermediate, diimine (DI_{MAG}). It implies that the cross reactions in MEA-AS-GL mixture are thermodynamical favorable. Therefore, the formation and propagation of chromophores in MEA-AS-GL mixture also proceed via NA reactions, which is the key route for the formation of BrC chromophores.

As shown in Fig. 3c, no bicyclic IML compounds are produced in MEA-AS-GL mixture because the precursors of bicyclic IML compound (i.e., imidazole-2-carboxaldehyde) is fully hydrated under more acidic condition than AS-GL mixture (see pH values in Table S2). It leads to the formation of N-glyoxal substituted imidazole (i.e., GI_{MAG}) instead of bicyclic IML compounds. The similar phenomenon is also found in the previous studies (Ackendorf et al., 2017; Kampf et al., 2012; Yu et al., 2011) that bicyclic IML compounds are hardly yield from imidazole-2-carboxaldehyde in acidic condition. As discussed above, imidazole-based structural characteristics in chromophores are maintained in the presence of MEA, but the nucleophilicity of chromophores is reduced because the nucleophilic sites are occupied. Also, the positively charged quaternary amine salts (such as IC_{MEA} and GI_{MAG}) are also yield in MEA-GL and MEA-AS-GL mixtures, and thereby the chemical composition and optical properties of chromophores are affected.

3.3 Chemical reaction mechanism leading to BrC chromophores

As discussed above, the four-step NA reactions are the key pathways to form and propagate oligomers including intermediates and chromophores for three mixtures. Therefore, all possible pathways involved in the four key NA reactions of three mixtures are calculated using density functional theory. The corresponding PESs stablished by the M06-2X/6-311+G(3df,3pd)//M06-2X/6-311G(d,p) level are also presented in dotted boxes of Figs. 4-5. The optimized geometries of key stationary points, including transition states (TSs), intermediates, and products, are depicted in Figs. S9-S11 at the M06-2X/6-311G(d,p) level. We first performed quantum chemistry calculation to evaluated the direct nucleophilic attack of GL by MEA or AS, which proceeds a large activation energy ($\Delta G^{\ddagger}$) value of 6.3 or 8.6 kcal mol^{-1}, following by H-shift reaction to yield AHA_{MEA} or AHA_{AS}, with also a large $\Delta G^{\ddagger}$ value of 15.2 or 18.2 kcal mol^{-1} (see NA1a' and NA2a' in Fig. 4). The high $\Delta G^{\ddagger}$ values and large endothermicity of the direct NA reactions leading to AHA_{MEA} and AHA_{AS} imply that their occurrences are kinetically and thermodynamically hindered.

https://doi.org/10.5194/egusphere-2023-2662
Preprint. Discussion started: 20 November 2023

Hence, we explored the cationic oligomerization of chromophore formation under acidic condition, which involves three essential steps, (1) protonation and dehydration to form cationic intermediates (CIs) or carbenium ions (CBs), (2) nucleophilic attack of CIs or CBs by MEA and AS, and (3) formation of intermediates and chromophores by deprotonation or dehydration. As shown in Figs. 4-5, each pathway involved in the cationic-mediated reaction mechanism proceeds without a TS, except deprotonation of CIs, in line with the results of the previous studies (Ji et al., 2020; Ji et al., 2022). However, deprotonation of CIs by sulfate ion (SO_4^{2-}) possesses a negative $\Delta G^{\ddagger}$ value in this study, implying an approximate barrierless process of this kind of deprotonation.

For the first-step NA reaction (NA1a in Fig. 4) in MEA-GL mixture, the electrophilic cationic site of CB_{DL} is attacked by the nucleophilic -NH_2 group of MEA with the ΔG_r value of −40.3 kcal mol^{-1}. CB_{DL} is broadly produced from GL and reflected from the large particle growth and formation of IML products (Ji et al., 2020; Li et al., 2021). The deprotonation of $CI_{MEA}1$ possesses a negative $\Delta G^{\ddagger}$ value of −4.5 kcal mol^{-1}, and a pre-reactive complex is identified prior the corresponding TS (detailed in SI). Similarly, the other two NA1b and NA1c reactions (Fig. 4) also include protonation, dehydration, nucleophilic attack, and deprotonation to yield HA_{MEA} and PIC_{MEA}. Kinetic data listed in Table S3 show that the rate constants of most pathways involved in the NA1a-1b and NA2a-2c reactions fall in the range of ~10^9 M^{-1} s^{-1}. The similar results can be drawn for AS-GL mixture, suggesting that the electrostatic attraction is a significant factor to affect the NA reactions.

To further evaluate the cationic reaction mechanism, the natural bond orbital (NBO) analysis reveals that the N atom of NH_3 exhibits more negative charge (−1.1 e) relative to MEA (−0.9 e), suggesting the stronger electrostatic attraction between CB_{DL} and NH_3 to yield $CI_{AS}1$ in the first-step NA reaction (see NA1a and NA2a in Fig. 4). However, the second-step NA reaction between CB_{MEA} and MEA are promoted by MEA because the presence of MEA enhances the positive charge in CB_{MEA} (0.6 e), facilitating the electrostatic attraction (see NA1b and NA2b in Fig. 4). For the third-step NA reaction (see NA1c and NA2c in Fig. 4), due to the steric hindrance, the deprotonation of $CI_{MEA}8$ possesses a larger $\Delta G^{\ddagger}$ value relative to that of $CI_{AS}8$. Hence, the NA reactions are regulated by both electrostatic attraction and steric hindrance effect.

The fourth-step NA reactions in MEA-GL and AS-GL mixtures exhibit two distinct chemical reaction mechanisms in cyclization to yield N-heterocycles (see NA1d and NA2d in Fig. 4). The protonation of PIC_{MEA} and PIC_{AS} occurs at the hydroxyl group to form $CI_{MEA}9$ and $CI_{AS}9$. For MEA-GL mixture, the barrierless dehydration and cyclization of $CI_{MEA}9$ occur in one step to yield N-heterocycle (i.e., IC_{MEA}), with the total ΔG_r value of −78.6 kcal mol^{-1} (NA1d in Fig. 4a). However, for AS-GL mixture, the cyclization of PIC_{AS} to IC_{AS} includes protonation, dehydration, cyclization, and deprotonation. Note that cyclization and deprotonation proceed via two TSs in sequence, with the corresponding $\Delta G^{\ddagger}$ values of 3.9 and −0.6 kcal mol^{-1} (NA2d in Fig. 4b), respectively, forming IC_{AS}. As discussed above, cyclization in MEA-GL and AS-GL mixtures is the rate-limiting step to chromophore formation.

For MEA-AS-GL mixture, $AHA_{MEA/AS}$, and $ID_{MEA/AS}$ are yielded via the same first NA reactions (NA1a/2a) as MEA-GL and AS-GL mixtures. Also, the formation of $ID_{MEA/AS}$ proceeds via protonation and dehydration to form $CB_{MEA/AS}$. However, the second NA reaction includes the cross-NA reaction of CB_{MEA} with AS (NA3b-1) or CB_{AS} with MEA (NA3b-2) to produce extra oligomers (i.e., $HA_{MAG}1$ and $HA_{MAG}2$), in contrast to MEA-GL and AS-GL mixtures. Hence, the fate of $CB_{MEA/AS}$ is

https://doi.org/10.5194/egusphere-2023-2662
Preprint. Discussion started: 20 November 2023

dependent of the competition reaction between the pathways of self-NA reaction to form $HA_{MEA/AS}$ (NA1b/2b) and cross-NA reaction to yield $HA_{MAG}1/2$ (NA3b-1/2). The ΔG_r values of the cross-NA reactions to yield $HA_{MAG}1$ and $HA_{MAG}2$ are −30.3 and −30.4 kcal mol^{-1}, respectively, comparable with those of self-NA reactions. It suggests both NA reactions to form HAs are equally accessible. Subsequently, $HA_{MAG}1/2$ undergoes dehydration to form DI_{MAG}, further proceeds the third NA reaction to yield PIC_{MAG}, in line with the mechanisms of the third NA reactions for MEA-GL and AS-GL mixtures. The cyclization of $CI_{MAG}10$ (the fourth NA reaction) possesses with two successive TSs, similar to that of AS-GL mixture but different to that of MEA-GL mixture. The corresponding $\Delta G^{\ddagger}$ values are obtained as 5.0 and 1.6 kcal mol^{-1}, respectively, which are larger than those of AS-GL mixture. In summary, compared with the AS-containing mixtures, the presence of MEA provides the extra two branched chains in N atoms, which affect the natural charges and molecular steric hindrance of intermediates, to thereby facilitate the intramolecular interaction between N and C atoms to form SBrC chromophores.

4 Conclusions and atmospheric implications

BrC chromophores play an important role in the Earth's radiative balance, air quality and human health. However, the formation mechanisms of BrC chromophores are not fully understood, hindering a comprehensive assessment of BrC chromophores on atmospheric chemistry and environmental impacts. Hence, using combined theoretical and experimental methods, we investigated the aqueous chemistry of typical RNCs with GL and evaluated the impact of typical multifunctional RNCs on the formation of BrC chromophores. Experimental studies show that the MAC values of chromophores are affected by the initial pH value for AS-GL, MEA-GL and MEA-AS-GL mixtures, and the growth rates of chromophores are enhanced in the presence of MEA. The optical properties of chromophores are regulated by monocyclic and bicyclic IML compounds in AS-GL mixture but by monocyclic IML compounds in MEA-containing mixtures (i.e., MEA-GL and MEA-AS-GL). Combined with the results of quantum chemical calculations, chromophore formation is characterized by nucleophilic addition with large exothermicity and strong electrostatic attraction among the MEA-derived intermediates, which are also enhanced by MEA.

In addition, to simply evaluate the impacts of MEA and AS on chromosphere formation in the aqueous aerosols and fog/cloud droplets, the dynamics process of GL from gas to aqueous phase was carried out (Fig. S12). The free energy difference reflects whether the liquid particles with MEA and AS (denoted as MEA and AS particles) prefer to adsorb and accommodate GL. As shown in Fig. S12, a larger decrease in the free energy (−3.7 kcal mol^{-1}) occurs when GL approaches the interface of the MEA particle relative to the AS particle, indicating a thermodynamically favorable process. Subsequently, the stabilized GL enters into the interior region of the MEA and AS particles, with slightly endothermic (1.6 and 2.4 kcal mol^{-1}). A smaller free energy difference from the interface into the interior region of the MEA particle implies that the interfacial GL is more readily promoted to enter the interior region of the particle when the particles contain MEA compared with AS. Hence, the interfacial and interior attraction on the MEA particle is more pronounced for small α-dicarbonyls, to facilitate the further engagement in the aqueous-phase reactions with RNCs in the particle.

https://doi.org/10.5194/egusphere-2023-2662
Preprint. Discussion started: 20 November 2023

Formation of SBrC from multifunctional RNCs and small α-dicarbonyls occurs widely on aqueous aerosols and fog/cloud droplets under typical atmospheric conditions. Compared with the ubiquitous coexistence between AS and small α-dicarbonyls from global aerosol measurement, SBrC aerosol formation from multifunctional RNC mixtures should be paid attention to during serious haze formation in China because of their atmospheric reactivities and non-negligible concentrations. Our results also imply that SBrC aerosols, if formed from the aqueous reactions between MEA and GL, likely contribute to atmospheric warming because the presence of MEA enhances the MACs of the mixture. Hence, recognition of this aerosol formation mechanism in the radiative transfer atmospheric model is needed, reparenting a possible missing source for BrC formation on urban, regional and global scales.

Data availability. All raw data can be provided by the corresponding authors upon request.

Supplement. The supplement related to this article is available on the EGU Publications website.

Author contributions. YMJ and ZS designed the research; YMJ, ZS, RZM, and WJL performed the research; YJ, ZS, WJL, JXW, QJS, YXL, LG, LLX, YPG, GYL, and TCA analyzed the data; YMJ and ZS wrote the paper. YMJ, YXL, YPG, GYL, and TCA reviewed and edited the paper.

Competing interests. The contact author has declared that neither they nor their co-authors have any competing interests.

Disclaimer. Publisher's note: Copernicus Publications remains neutral with regard to jurisdictional claims in published maps and institutional affiliations.

Financial support. This work was financially supported by National Natural Science Foundation of China (grant nos. 42077189 and 42020104001), Guangdong Basic and Applied Basic Research Foundation (Grant Nos. 2019B151502064), Local Innovative and Research Teams Project of Guangdong Pearl River Talents Program (Grant Nos. 2017BT01Z032), and Guangdong Provincial Key R&D Program (Grant Nos. 2022-GDUT-A0007).

Review statement. This paper was edited and reviewed by two anonymous referees.

References

Ackendorf, J. M., Ippolito, M. G., and Galloway, M. M.: pH Dependence of the Imidazole-2-carboxaldehyde Hydration Equilibrium: Implications for Atmospheric Light Absorbance, Environ. Sci. Technol. Lett., 4, 551-555, https://doi.org/10.1021/acs.estlett.7b00486, 2017.

Aiona, P. K., Lee, H. J., Leslie, R., Lin, P., Laskin, A., Laskin, J., and Nizkorodov, S. A.: Photochemistry of Products of the Aqueous Reaction of Methylglyoxal with Ammonium Sulfate, ACS Earth Space Chem., 1, 522-532,

https://doi.org/10.5194/egusphere-2023-2662
Preprint. Discussion started: 20 November 2023

https://doi.org/10.1021/acsearthspacechem.7b00075, 2017.

An, Z., Huang, R. J., Zhang, R., Tie, X., Li, G., Cao, J., Zhou, W., Shi, Z., Han, Y., Gu, Z., and Ji, Y.: Severe haze in northern China: A synergy of anthropogenic emissions and atmospheric processes, Proc. Natl. Acad. Sci. U. S. A., 116, 8657-8666, https://doi.org/10.1073/pnas.1900125116, 2019.

Chen, Y. and Bond, T. C.: Light absorption by organic carbon from wood combustion, Atmos. Chem. Phys., 10, 1773-1787, https://doi.org/DOI 10.5194/acp-10-1773-2010, 2010.

Collins, F. C. and Kimball, G. E.: Diffusion-controlled reaction rates, J. Colloid Sci., 4, 425-437, https://doi.org/https://doi.org/10.1016/0095-8522(49)90023-9, 1949.

Corbin, J. C., Czech, H., Massabò, D., de Mongeot, F. B., Jakobi, G., Liu, F., Lobo, P., Mennucci, C., Mensah, A. A., Orasche, J., Pieber, S. M., Prévôt, A. S. H., Stengel, B., Tay, L. L., Zanatta, M., Zimmermann, R., El Haddad, I., and Gysel, M.: Infrared-absorbing carbonaceous tar can dominate light absorption by marine-engine exhaust, npj Clim. Atmos. Sci., 2, https://doi.org/10.1038/s41612-019-0069-5, 2019.

De Haan, D. O., Tolbert, M. A., and Jimenez, J. L.: Atmospheric condensed-phase reactions of glyoxal with methylamine, Geophys. Res. Lett., 36, https://doi.org/10.1029/2009gl037441, 2009a.

De Haan, D. O., Corrigan, A. L., Smith, K. W., Stroik, D. R., Turley, J. J., Lee, F. E., Tolbert, M. A., Jimenez, J. L., Cordova, K. E., and Ferrell, G. R.: Secondary Organic Aerosol-Forming Reactions of Glyoxal with Amino Acids, Environ. Sci. Technol., 43, 2818-2824, https://doi.org/10.1021/es803534f, 2009b.

De Haan, D. O., Hawkins, L. N., Jansen, K., Welsh, H. G., Pednekar, R., de Loera, A., Jimenez, N. G., Tolbert, M. A., Cazaunau, M., Gratien, A., Bergé, A., Pangui, E., Formenti, P., and Doussin, J.-F.: Glyoxal's impact on dry ammonium salts: fast and reversible surface aerosol browning, Atmos. Chem. Phys., 20, 9581-9590, https://doi.org/10.5194/acp-20-9581-2020, 2020.

De Haan, D. O., Tapavicza, E., Riva, M., Cui, T., Surratt, J. D., Smith, A. C., Jordan, M. C., Nilakantan, S., Almodovar, M., Stewart, T. N., de Loera, A., De Haan, A. C., Cazaunau, M., Gratien, A., Pangui, E., and Doussin, J. F.: Nitrogen-Containing, Light-Absorbing Oligomers Produced in Aerosol Particles Exposed to Methylglyoxal, Photolysis, and Cloud Cycling, Environ. Sci. Technol., 52, 4061-4071, https://doi.org/10.1021/acs.est.7b06105, 2018.

De Haan, D. O., Pajunoja, A., Hawkins, L. N., Welsh, H. G., Jimenez, N. G., De Loera, A., Zauscher, M., Andretta, A. D., Joyce, B. W., De Haan, A. C., Riva, M., Cui, T., Surratt, J. D., Cazaunau, M., Formenti, P., Gratien, A., Pangui, E., and Doussin, J.-F.: Methylamine's Effects on Methylglyoxal-Containing Aerosol: Chemical, Physical, and Optical Changes, ACS Earth Space Chem., 3, 1706-1716, https://doi.org/10.1021/acsearthspacechem.9b00103, 2019.

Evans, M. G. and Polanyi, M.: Some applications of the transition state method to the calculation of reaction velocities, especially in solution, Trans. Faraday Soc., 31, 875-894, https://doi.org/10.1039/TF9353100875, 1935.

Eyring, H.: The Activated Complex in Chemical Reactions, J. Chem. Phys., 3, 107-115, https://doi.org/10.1063/1.1749604, 1935.

Fu, T.-M., Jacob, D. J., Wittrock, F., Burrows, J. P., Vrekoussis, M., and Henze, D. K.: Global budgets of atmospheric glyoxal and methylglyoxal, and implications for formation of secondary organic aerosols, J. Geophys. Res., 113,

https://doi.org/10.5194/egusphere-2023-2662
Preprint. Discussion started: 20 November 2023

https://doi.org/10.1029/2007jd009505, 2008.

Galano, A. and Alvarez-Idaboy, J. R.: Guanosine + OH Radical Reaction in Aqueous Solution: A Reinterpretation of the UV−vis Data Based on Thermodynamic and Kinetic Calculations, Org. Lett., 11, 5114-5117, https://doi.org/10.1021/ol901862h, 2009.

Galloway, M. M., Chhabra, P. S., Chan, A. W. H., Surratt, J. D., Flagan, R. C., Seinfeld, J. H., and Keutsch, F. N.: Glyoxal uptake on ammonium sulphate seed aerosol: reaction products and reversibility of uptake under dark and irradiated conditions, Atmos. Chem. Phys., 9, 3331-3345, https://doi.org/10.5194/acp-9-3331-2009, 2009.

Gao, Y., Ji, Y., Li, G., and An, T.: Mechanism, kinetics and toxicity assessment of OH-initiated transformation of triclosan in aquatic environments, Water Res., 49, 360-370, https://doi.org/10.1016/j.watres.2013.10.027, 2014.

Gao, Y., Ji, Y., Li, G., Mai, B., and An, T.: Bioaccumulation and ecotoxicity increase during indirect photochemical transformation of polycyclic musk tonalide: A modeling study, Water Res., 105, 47-55, https://doi.org/10.1016/j.watres.2016.08.055, 2016.

Ge, X., Wexler, A. S., and Clegg, S. L.: Atmospheric amines – Part I. A review, Atmos. Environ., 45, 524-546, https://doi.org/10.1016/j.atmosenv.2010.10.012, 2011.

George, C., Ammann, M., D'Anna, B., Donaldson, D. J., and Nizkorodov, S. A.: Heterogeneous photochemistry in the atmosphere, Chem. Rev., 115, 4218-4258, https://doi.org/10.1021/cr500648z, 2015.

Gomez, M. E., Lin, Y., Guo, S., and Zhang, R.: Heterogeneous Chemistry of Glyoxal on Acidic Solutions. An Oligomerization Pathway for Secondary Organic Aerosol Formation, J. Phys. Chem. A, 119, 4457-4463, https://doi.org/10.1021/jp509916r, 2015.

Hamilton, J. F., Baeza-Romero, M. T., Finessi, E., Rickard, A. R., Healy, R. M., Peppe, S., Adams, T. J., Daniels, M. J. S., Ball, S. M., Goodall, I. C. A., Monks, P. S., Borrás, E., and Muñoz, A.: Online and offline mass spectrometric study of the impact of oxidation and ageing on glyoxal chemistry and uptake onto ammonium sulfate aerosols, Faraday Discuss., 165, https://doi.org/10.1039/c3fd00051f, 2013.

Hawkins, L. N., Welsh, H. G., and Alexander, M. V.: Evidence for pyrazine-based chromophores in cloud water mimics containing methylglyoxal and ammonium sulfate, Atmos. Chem. Phys., 18, 12413-12431, https://doi.org/10.5194/acp-18-12413-2018, 2018.

Huang, X., Deng, C., Zhuang, G., Lin, J., and Xiao, M.: Quantitative analysis of aliphatic amines in urban aerosols based on online derivatization and high performance liquid chromatography, Environ. Sci.: Processes Impacts, 18, 796-801, https://doi.org/10.1039/c6em00197a, 2016.

Ji, Y., Shi, Q., Ma, X., Gao, L., Wang, J., Li, Y., Gao, Y., Li, G., Zhang, R., and An, T.: Elucidating the critical oligomeric steps in secondary organic aerosol and brown carbon formation, Atmos. Chem. Phys., 22, 7259-7271, https://doi.org/10.5194/acp-22-7259-2022, 2022.

Ji, Y., Shi, Q., Li, Y., An, T., Zheng, J., Peng, J., Gao, Y., Chen, J., Li, G., Wang, Y., Zhang, F., Zhang, A. L., Zhao, J., Molina, M. J., and Zhang, R.: Carbenium ion-mediated oligomerization of methylglyoxal for secondary organic aerosol formation,

https://doi.org/10.5194/egusphere-2023-2662
Preprint. Discussion started: 20 November 2023

Proc. Natl. Acad. Sci. U. S. A., 117, 13294-13299, https://doi.org/10.1073/pnas.1912235117, 2020.

Ji, Y., Zhao, J., Terazono, H., Misawa, K., Levitt, N. P., Li, Y., Lin, Y., Peng, J., Wang, Y., Duan, L., Pan, B., Zhang, F., Feng, X., An, T., Marrero-Ortiz, W., Secrest, J., Zhang, A. L., Shibuya, K., Molina, M. J., and Zhang, R.: Reassessing the atmospheric oxidation mechanism of toluene, Proc. Natl. Acad. Sci. U. S. A., 114, 8169, https://doi.org/10.1073/pnas.1705463114, 2017.

Jorgensen, W. L., Maxwell, D. S., and Tirado-Rives, J.: Development and Testing of the OPLS All-Atom Force Field on Conformational Energetics and Properties of Organic Liquids, J. Am. Chem. Soc., 118, 11225-11236, https://doi.org/10.1021/ja9621760, 1996.

Kampf, C. J., Jakob, R., and Hoffmann, T.: Identification and characterization of aging products in the glyoxal/ammonium sulfate system – implications for light-absorbing material in atmospheric aerosols, Atmos. Chem. Phys., 12, 6323-6333, https://doi.org/10.5194/acp-12-6323-2012, 2012.

Kampf, C. J., Filippi, A., Zuth, C., Hoffmann, T., and Opatz, T.: Secondary brown carbon formation via the dicarbonyl imine pathway: nitrogen heterocycle formation and synergistic effects, Phys. Chem. Chem. Phys., 18, 18353-18364, https://doi.org/10.1039/c6cp03029g, 2016.

Karl, M., Wright, R. F., Berglen, T. F., and Denby, B.: Worst case scenario study to assess the environmental impact of amine emissions from a CO2 capture plant, Int. J. Greenh. Gas Control, 5, 439-447, https://doi.org/10.1016/j.ijggc.2010.11.001, 2011.

Kasthuriarachchi, N. Y., Rivellini, L. H., Adam, M. G., and Lee, A. K. Y.: Light Absorbing Properties of Primary and Secondary Brown Carbon in a Tropical Urban Environment, Environ. Sci. Technol., 54, 10808-10819, https://doi.org/10.1021/acs.est.0c02414, 2020.

Kumar, S., Rosenberg, J. M., Bouzida, D., Swendsen, R. H., and Kollman, P. A.: The weighted histogram analysis method for free-energy calculations on biomolecules. I. The method, J. Comput. Chem., 13, 1011-1021, https://doi.org/10.1002/jcc.540130812, 1992.

Laskin, A., Laskin, J., and Nizkorodov, S. A.: Chemistry of atmospheric brown carbon, Chem. Rev., 115, 4335-4382, https://doi.org/10.1021/cr5006167, 2015.

Lee, A. K. Y., Zhao, R., Li, R., Liggio, J., Li, S.-M., and Abbatt, J. P. D.: Formation of Light Absorbing Organo-Nitrogen Species from Evaporation of Droplets Containing Glyoxal and Ammonium Sulfate, Environ. Sci. Technol., 47, 12819-12826, https://doi.org/10.1021/es402687w, 2013.

Lee, H. J., Aiona, P. K., Laskin, A., Laskin, J., and Nizkorodov, S. A.: Effect of solar radiation on the optical properties and molecular composition of laboratory proxies of atmospheric brown carbon, Environ. Sci. Technol., 48, 10217-10226, https://doi.org/10.1021/es502515r, 2014.

Leontyev, I. and Stuchebrukhov, A.: Accounting for electronic polarization in non-polarizable force fields, Phys. Chem. Chem. Phys., 13, 2613-2626, https://doi.org/10.1039/c0cp01971b, 2011.

Li, X., Sun, N., Jin, Q., Zhao, Z., Wang, L., Wang, Q., Gu, X., Li, Y., and Liu, X.: Light absorption properties of black and brown carbon in winter over the North China Plain: Impacts of regional biomass burning, Atmos. Environ., 278, https://doi.org/10.1016/j.atmosenv.2022.119100, 2022.

https://doi.org/10.5194/egusphere-2023-2662
Preprint. Discussion started: 20 November 2023

Li, Y., Ji, Y., Zhao, J., Wang, Y., Shi, Q., Peng, J., Wang, Y., Wang, C., Zhang, F., Wang, Y., Seinfeld, J. H., and Zhang, R.: Unexpected Oligomerization of Small alpha-Dicarbonyls for Secondary Organic Aerosol and Brown Carbon Formation, Environ. Sci. Technol., 55, 4430-4439, https://doi.org/10.1021/acs.est.0c08066, 2021.

Lin, P., Laskin, J., Nizkorodov, S. A., and Laskin, A.: Revealing Brown Carbon Chromophores Produced in Reactions of Methylglyoxal with Ammonium Sulfate, Environ. Sci. Technol., 49, 14257-14266, https://doi.org/10.1021/acs.est.5b03608, 2015.

Liu, D., He, C., Schwarz, J. P., and Wang, X.: Lifecycle of light-absorbing carbonaceous aerosols in the atmosphere, npj Clim. Atmos. Sci., 3, 40, https://doi.org/10.1038/s41612-020-00145-8, 2020.

M. J.Frisch, G. W. T., H. B.Schlegel, G. E.Scuseria, M. A.Robb, J. R.Cheeseman, G.Scalmani, V.Barone, B.Mennucci, G. A.Petersson, H.Nakatsuji, M.Caricato, X.Li, H. P.Hratchian, A. F.Izmaylov, J.Bloino, G.Zheng, J. L.Sonnenberg, M.Hada, M.Ehara, K.Toyota, R.Fukuda, J.Hasegawa, M.Ishida, T.Nakajima, Y.Honda, O.Kitao, H.Nakai, T.Vreven, J. A.Montgomery, Jr., J. E.Peralta, F.Ogliaro, M.Bearpark, J. J.Heyd, E.Brothers, K. N.Kudin, V. N.Staroverov, T.Keith, R.Kobayashi, J.Normand, K.Raghavachari, A.Rendell, J. C.Burant, S. S.Iyengar, J.Tomasi, M.Cossi, N.Rega, J. M.Millam, M.Klene, J. E.Knox, J. B.Cross, V.Bakken, C.Adamo, J.Jaramillo, R.Gomperts, R. E.Stratmann, O.Yazyev, A. J.Austin, R.Cammi, C.Pomelli, J. W.Ochterski, R. L.Martin, K.Morokuma, V. G.Zakrzewski, G. A.Voth, P.Salvador, J. J.Dannenberg, S.Dapprich, A. D.Daniels, O.Farkas, J. B.Foresman, J. V.Ortiz, J.Cioslowski and D. J.Fox: Gaussian 09, Revision D.01, Gaussian, Inc., Wallingford CT, 2013, 2013.

Marenich, A. V., Cramer, C. J., and Truhlar, D. G.: Universal Solvation Model Based on Solute Electron Density and on a Continuum Model of the Solvent Defined by the Bulk Dielectric Constant and Atomic Surface Tensions, J. Phys. Chem. B, 113, 6378-6396, https://doi.org/10.1021/jp810292n, 2009.

Marrero-Ortiz, W., Hu, M., Du, Z., Ji, Y., Wang, Y., Guo, S., Lin, Y., Gomez-Hermandez, M., Peng, J., Li, Y., Secrest, J., Zamora, M. L., Wang, Y., An, T., and Zhang, R.: Formation and Optical Properties of Brown Carbon from Small α-Dicarbonyls and Amines, Environ. Sci. Technol., 53, 117-126, https://doi.org/10.1021/acs.est.8b03995, 2018.

Martins-Costa, M. T., Anglada, J. M., Francisco, J. S., and Ruiz-Lopez, M. F.: Reactivity of volatile organic compounds at the surface of a water droplet, J. Am. Chem. Soc., 134, 11821-11827, https://doi.org/10.1021/ja304971e, 2012.

Moise, T., Flores, J. M., and Rudich, Y.: Optical properties of secondary organic aerosols and their changes by chemical processes, Chem. Rev., 115, 4400-4439, https://doi.org/10.1021/cr5005259, 2015.

Mosallanejad, S., Oluwoye, I., Altarawneh, M., Gore, J., and Dlugogorski, B. Z.: Interfacial and bulk properties of concentrated solutions of ammonium nitrate, Phys. Chem. Chem. Phys., 22, 27698-27712, https://doi.org/10.1039/d0cp04874g, 2020.

Myriokefalitakis, S., Vrekoussis, M., Tsigaridis, K., Wittrock, F., Richter, A., Brühl, C., Volkamer, R., Burrows, J. P., and Kanakidou, M.: The influence of natural and anthropogenic secondary sources on the glyoxal global distribution, Atmos. Chem. Phys., 8, 4965-4981, https://doi.org/10.5194/acp-8-4965-2008, 2008.

Nie, W., Yan, C., Huang, D. D., Wang, Z., Liu, Y., Qiao, X., Guo, Y., Tian, L., Zheng, P., Xu, Z., Li, Y., Xu, Z., Qi, X., Sun, P., Wang, J., Zheng, F., Li, X., Yin, R., Dallenbach, K. R., Bianchi, F., Petäjä, T., Zhang, Y., Wang, M., Schervish, M., Wang, S.,

https://doi.org/10.5194/egusphere-2023-2662
Preprint. Discussion started: 20 November 2023

Qiao, L., Wang, Q., Zhou, M., Wang, H., Yu, C., Yao, D., Guo, H., Ye, P., Lee, S., Li, Y. J., Liu, Y., Chi, X., Kerminen, V.-M., Ehn, M., Donahue, N. M., Wang, T., Huang, C., Kulmala, M., Worsnop, D., Jiang, J., and Ding, A.: Secondary organic aerosol formed by condensing anthropogenic vapours over China's megacities, Nat. Geosci., 15, 255-261, https://doi.org/10.1038/s41561-022-00922-5, 2022.

Ning, A., Liu, L., Zhang, S., Yu, F., Du, L., Ge, M., and Zhang, X.: The critical role of dimethylamine in the rapid formation of iodic acid particles in marine areas, npj Clim. Atmos. Sci., 5, 92, https://doi.org/10.1038/s41612-022-00316-9, 2022.

Nozière, B., Dziedzic, P., and Córdova, A.: Products and Kinetics of the Liquid-Phase Reaction of Glyoxal Catalyzed by Ammonium Ions (NH4+), J. Phys. Chem. A, 113, 231-237, https://doi.org/10.1021/jp8078293, 2009.

Okuno, Y.: Theoretical Investigation of the Mechanism of the Baeyer-Villiger Reaction in Nonpolar Solvents, Chem. - Eur. J., 3, 212-218, https://doi.org/https://doi.org/10.1002/chem.19970030208, 1997.

Phillips, J. C., Braun, R., Wang, W., Gumbart, J., Tajkhorshid, E., Villa, E., Chipot, C., Skeel, R. D., Kale, L., and Schulten, K.: Scalable molecular dynamics with NAMD, J. Comput. Chem., 26, 1781-1802, https://doi.org/10.1002/jcc.20289, 2005.

Powelson, M. H., Espelien, B. M., Hawkins, L. N., Galloway, M. M., and De Haan, D. O.: Brown carbon formation by aqueous-phase carbonyl compound reactions with amines and ammonium sulfate, Environ. Sci. Technol., 48, 985-993, https://doi.org/10.1021/es4038325, 2014.

Puxty, G., Rowland, R., Allport, A., Yang, Q., Bown, M., Burns, R., Maeder, M., and Attalla, M.: Carbon Dioxide Postcombustion Capture: A Novel Screening Study of the Carbon Dioxide Absorption Performance of 76 Amines, Environ. Sci. Technol., 43, 6427-6433, https://doi.org/10.1021/es901376a, 2009.

Sedehi, N., Takano, H., Blasic, V. A., Sullivan, K. A., and De Haan, D. O.: Temperature- and pH-dependent aqueous-phase kinetics of the reactions of glyoxal and methylglyoxal with atmospheric amines and ammonium sulfate, Atmos. Environ., 77, 656-663, https://doi.org/10.1016/j.atmosenv.2013.05.070, 2013.

Shapiro, E. L., Szprengiel, J., Sareen, N., Jen, C. N., Giordano, M. R., and McNeill, V. F.: Light-absorbing secondary organic material formed by glyoxal in aqueous aerosol mimics, Atmos. Chem. Phys., 9, 2289-2300, https://doi.org/10.5194/acp-9-2289-2009, 2009.

Shen, J., Xie, H.-B., Elm, J., Ma, F., Chen, J., and Vehkamäki, H.: Methanesulfonic Acid-driven New Particle Formation Enhanced by Monoethanolamine: A Computational Study, Environ. Sci. Technol., 53, 14387-14397, https://doi.org/10.1021/acs.est.9b05306, 2019.

Shi, Q., Zhang, W., Ji, Y., Wang, J., Qin, D., Chen, J., Gao, Y., Li, G., and An, T.: Enhanced uptake of glyoxal at the acidic nanoparticle interface: implications for secondary organic aerosol formation, Environ. Sci.: Nano, 7, 1126-1135, https://doi.org/10.1039/d0en00016g, 2020.

Srivastava, D., Vu, T. V., Tong, S., Shi, Z., and Harrison, R. M.: Formation of secondary organic aerosols from anthropogenic precursors in laboratory studies, npj Clim. Atmos. Sci., 5, https://doi.org/10.1038/s41612-022-00238-6, 2022.

Torrie, G. M. and Valleau, J. P.: Nonphysical sampling distributions in Monte Carlo free-energy estimation: Umbrella sampling, J. Comput. Phys., 23, 187-199, https://doi.org/https://doi.org/10.1016/0021-9991(77)90121-8, 1977.

https://doi.org/10.5194/egusphere-2023-2662
Preprint. Discussion started: 20 November 2023

Trainic, M., Riziq, A. A., Lavi, A., and Rudich, Y.: Role of interfacial water in the heterogeneous uptake of glyoxal by mixed glycine and ammonium sulfate aerosols, J. Phys. Chem. A, 116, 5948-5957, https://doi.org/10.1021/jp2104837, 2012.

Tuccella, P., Curci, G., Pitari, G., Lee, S., and Jo, D. S.: Direct Radiative Effect of Absorbing Aerosols: Sensitivity to Mixing State, Brown Carbon, and Soil Dust Refractive Index and Shape, J. Geophys. Res.: Atmos., 125, https://doi.org/10.1029/2019jd030967, 2020.

Wang, X., Heald, C. L., Liu, J., Weber, R. J., Campuzano-Jost, P., Jimenez, J. L., Schwarz, J. P., and Perring, A. E.: Exploring the observational constraints on the simulation of brown carbon, Atmos. Chem. Phys., 18, 635-653, https://doi.org/10.5194/acp-18-635-2018, 2018.

Wang, X., Hayeck, N., Brüggemann, M., Yao, L., Chen, H., Zhang, C., Emmelin, C., Chen, J., George, C., and Wang, L.: Chemical Characteristics of Organic Aerosols in Shanghai: A Study by Ultrahigh-Performance Liquid Chromatography Coupled With Orbitrap Mass Spectrometry, J. Geophys. Res.: Atmos., 122, 11,703-711,722, https://doi.org/10.1002/2017jd026930, 2017.

Yan, J., Wang, X., Gong, P., Wang, C., and Cong, Z.: Review of brown carbon aerosols: Recent progress and perspectives, Sci. Total Environ., 634, 1475-1485, https://doi.org/10.1016/j.scitotenv.2018.04.083, 2018.

Yang, Z., Tsona, N. T., George, C., and Du, L.: Nitrogen-Containing Compounds Enhance Light Absorption of Aromatic-Derived Brown Carbon, Environ. Sci. Technol., 56, 4005-4016, https://doi.org/10.1021/acs.est.1c08794, 2022.

Yu, G., Bayer, A. R., Galloway, M. M., Korshavn, K. J., Fry, C. G., and Keutsch, F. N.: Glyoxal in aqueous ammonium sulfate solutions: products, kinetics and hydration effects, Environ. Sci. Technol., 45, 6336-6342, https://doi.org/10.1021/es200989n, 2011.

Yuan, W., Huang, R.-J., Shen, J., Wang, K., Yang, L., Wang, T., Gong, Y., Cao, W., Guo, J., Ni, H., Duan, J., and Hoffmann, T.: More water-soluble brown carbon after the residential "coal-to-gas" conversion measure in urban Beijing, npj Clim. Atmos. Sci., 6, https://doi.org/10.1038/s41612-023-00355-w, 2023.

Yuan, W., Huang, R.-J., Yang, L., Guo, J., Chen, Z., Duan, J., Wang, T., Ni, H., Han, Y., Li, Y., Chen, Q., Chen, Y., Hoffmann, T., and O'Dowd, C.: Characterization of the light-absorbing properties, chromophore composition and sources of brown carbon aerosol in Xi'an, northwestern China, Atmos. Chem. Phys., 20, 5129-5144, https://doi.org/10.5194/acp-20-5129-2020, 2020.

Zhang, A., Wang, Y., Zhang, Y., Weber, R. J., Song, Y., Ke, Z., and Zou, Y.: Modeling the global radiative effect of brown carbon: a potentially larger heating source in the tropical free troposphere than black carbon, Atmos. Chem. Phys., 20, 1901-1920, https://doi.org/10.5194/acp-20-1901-2020, 2020.

Zhang, W., Ji, Y., Li, G., Shi, Q., and An, T.: The heterogeneous reaction of dimethylamine/ammonia with sulfuric acid to promote the growth of atmospheric nanoparticles, Environ. Sci.: Nano, 6, 2767-2776, https://doi.org/10.1039/c9en00619b, 2019.

Zhang, X., Tong, S., Jia, C., Zhang, W., Wang, Z., Tang, G., Hu, B., Liu, Z., Wang, L., Zhao, P., Pan, Y., and Ge, M.: Elucidating HONO formation mechanism and its essential contribution to OH during haze events, npj Clim. Atmos. Sci., 6, 55, https://doi.org/10.1038/s41612-023-00371-w, 2023.

https://doi.org/10.5194/egusphere-2023-2662
Preprint. Discussion started: 20 November 2023

524 Zhao, R., Lee, A. K. Y., Huang, L., Li, X., Yang, F., and Abbatt, J. P. D.: Photochemical processing of aqueous atmospheric
525 brown carbon, Atmos. Chem. Phys., 15, 6087-6100, https://doi.org/10.5194/acp-15-6087-2015, 2015.
526 Zhao, Y. and Truhlar, D. G.: The M06 suite of density functionals for main group thermochemistry, thermochemical kinetics,
527 noncovalent interactions, excited states, and transition elements: two new functionals and systematic testing of four M06-class
528 functionals and 12 other functionals, Theor. Chem. Acc., 120, 215-241, https://doi.org/10.1007/s00214-007-0310-x, 2007.
529

https://doi.org/10.5194/egusphere-2023-2662
Preprint. Discussion started: 20 November 2023

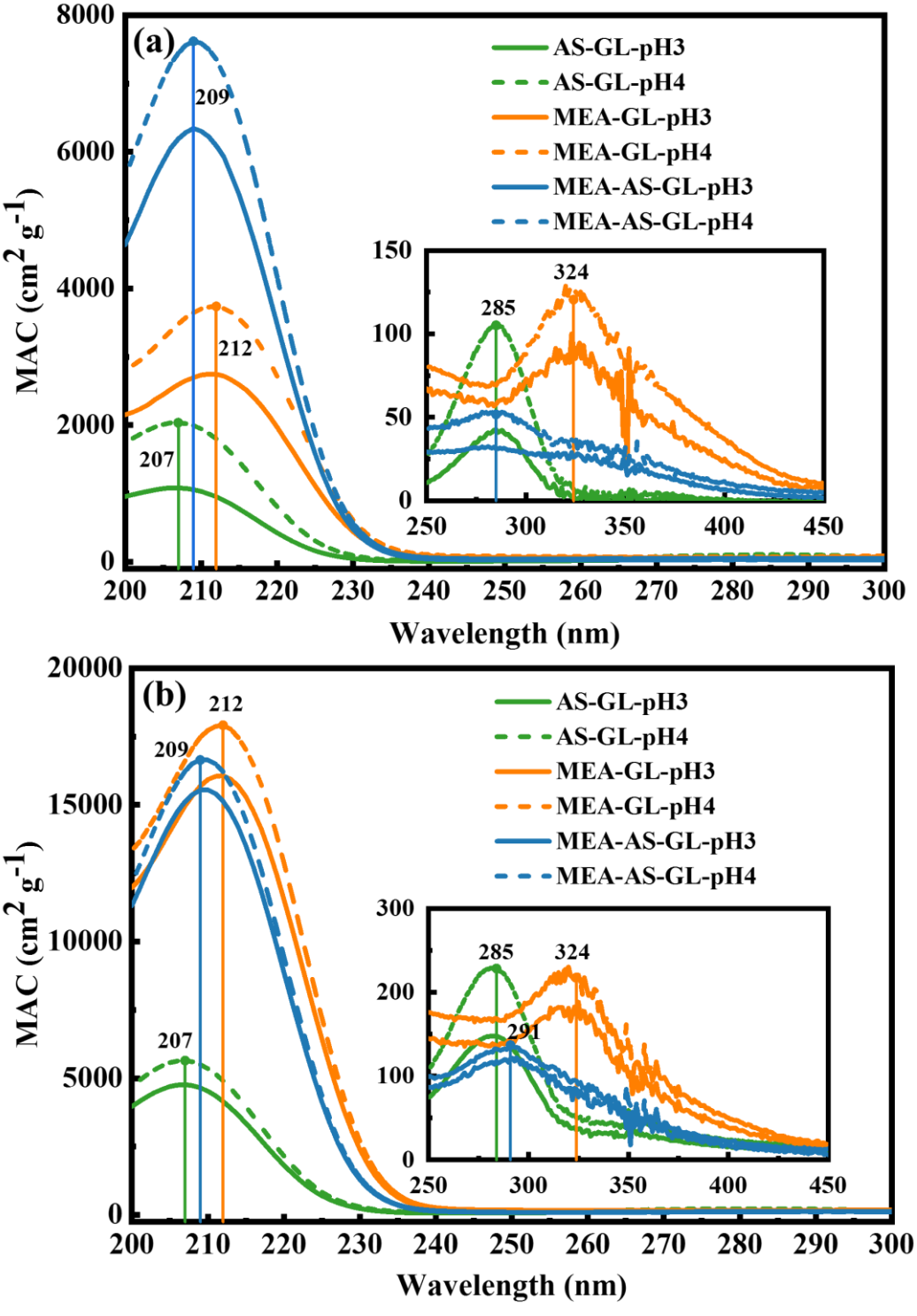

530

531 **Figure 1: The MAC values for AS-GL, MEA-GL and MEA-AS-GL mixtures at the initial pH of 3 and 4 at 1d (a) and 15d (b).**

https://doi.org/10.5194/egusphere-2023-2662
Preprint. Discussion started: 20 November 2023

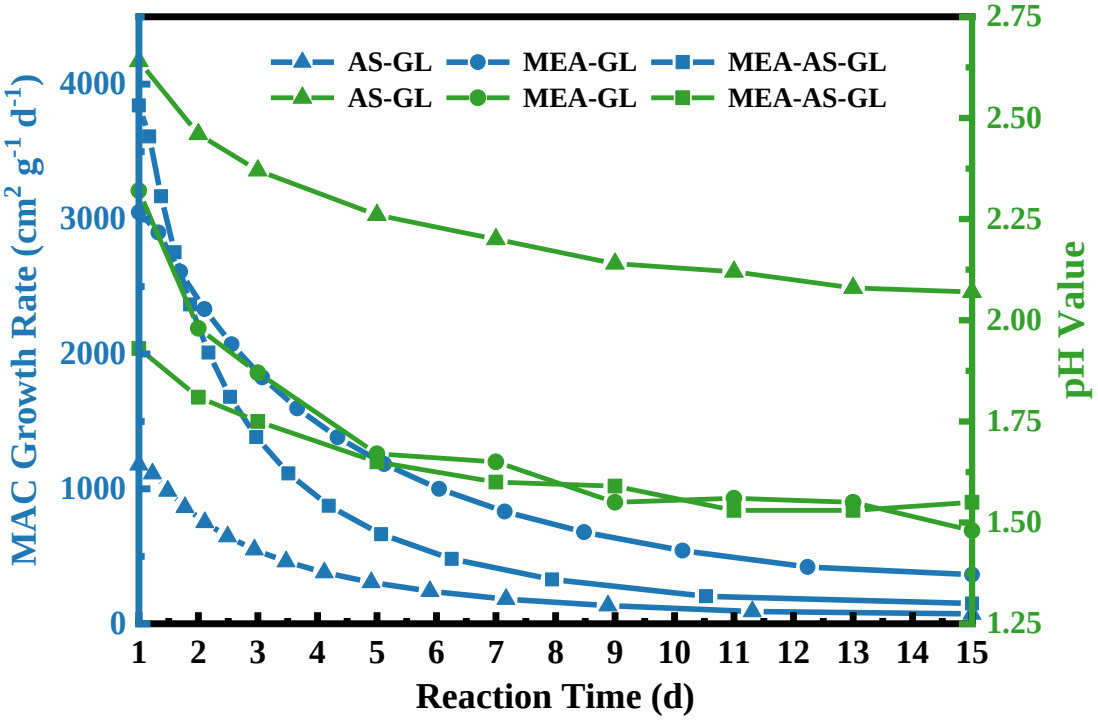

Figure 2: Dependence of the growth rates (blue line) and pH values (green line) on reaction time for AS-GL, MEA-GL and MEA-AS-GL mixtures.

https://doi.org/10.5194/egusphere-2023-2662
Preprint. Discussion started: 20 November 2023

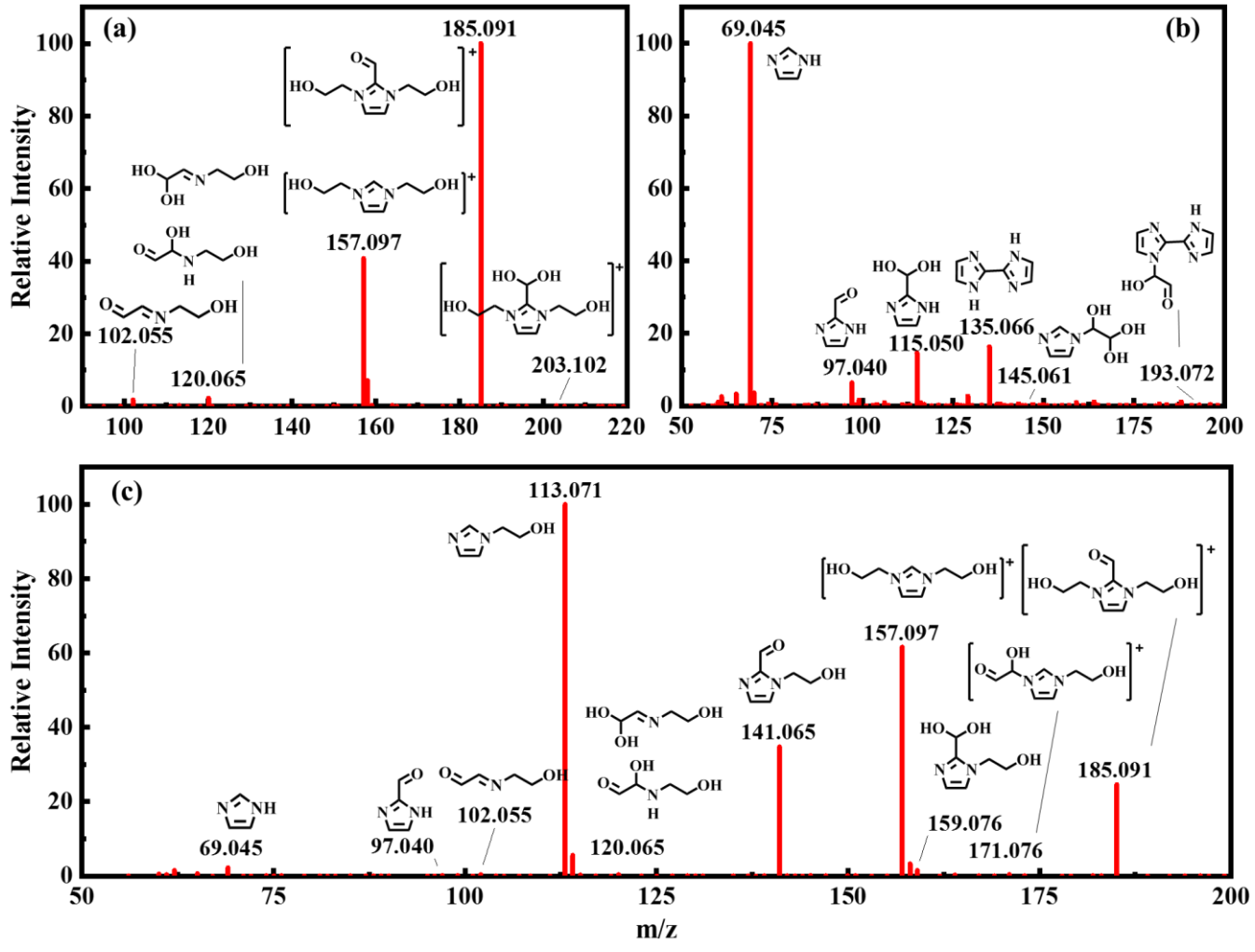

Figure 3: Mass spectra monitoring of chromophores for (a) MEA-GL (b) AS-GL and (c) MEA-AS-GL mixtures.

https://doi.org/10.5194/egusphere-2023-2662
Preprint. Discussion started: 20 November 2023

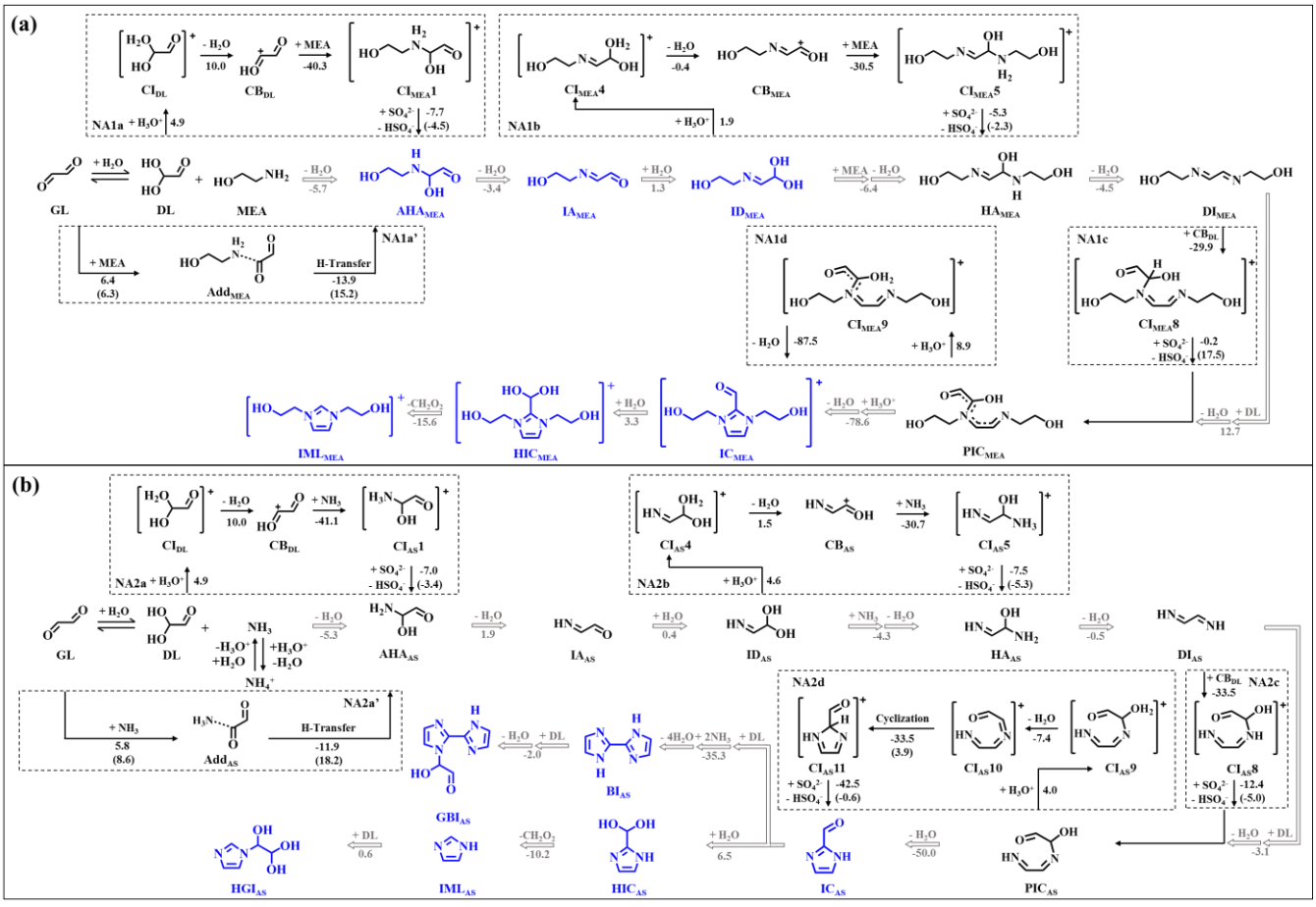

Figure 4: Possible pathways leading to chromophores for (a) MEA-GL and (b) AS-GL mixtures (oriented by gray arrows). Detailed PESs of the four NA reactions are presented in dotted boxes. The number denotes the values of ΔG_r and $\Delta G^{\ddagger}$ (in brackets) for each reaction step (in kcal mol^{-1}), and all energies are relative to the corresponding reactants.

https://doi.org/10.5194/egusphere-2023-2662
Preprint. Discussion started: 20 November 2023

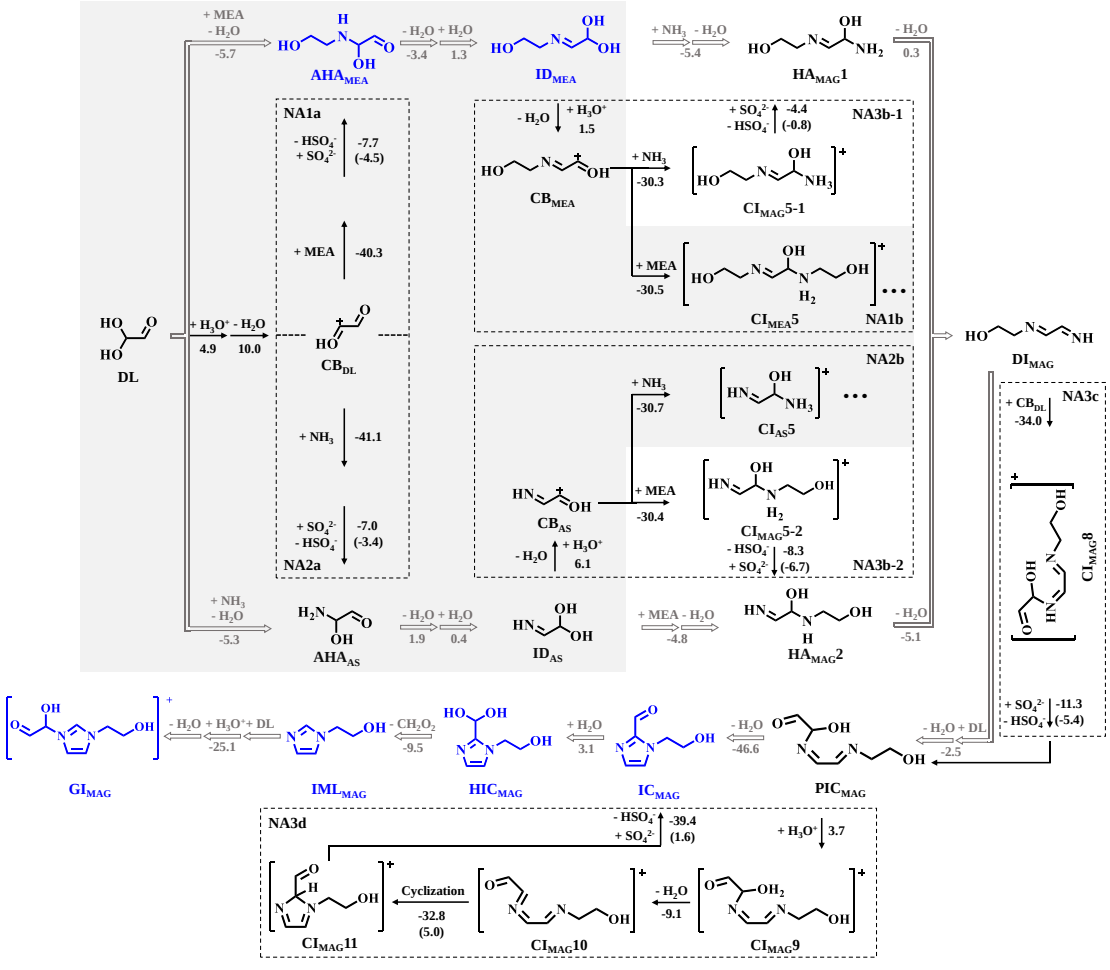

Figure 5: Possible pathways leading to chromophores for MEA-AS-GL mixture (oriented by gray arrows). Detailed PESs of the four NA reactions are presented in dotted box. The shaded area is the overlapping part with the pathways of MEA-GL and AS-GL mixtures. The number denotes the value of ΔG_r and $\Delta G^{\ddagger}$ (in brackets) for each reaction step (in kcal mol^{-1}), and all energies are relative to the corresponding reactants.